

# UC Berkeley

## UC Berkeley Previously Published Works

### Title

Dissociative photoionization of glycerol and its dimer occurs predominantly via a ternary hydrogen-bridged ion-molecule complex.

### Permalink

<https://escholarship.org/uc/item/7jf7s10b>

### Journal

Journal of the American Chemical Society, 135(38)

### ISSN

0002-7863

### Authors

Bell, Franziska  
Ruan, Qiao N  
Golan, Amir  
[et al.](#)

### Publication Date

2013-09-01

### DOI

10.1021/ja405511v

Peer reviewed

This document is confidential and is proprietary to the American Chemical Society and its authors. Do not copy or disclose without written permission. If you have received this item in error, notify the sender and delete all copies.

**Dissociative Photoionization of Glycerol and its Dimer  
Occurs Predominantly via a Ternary Hydrogen-Bridged Ion-  
Molecule Complex**

Journal:	<i>Journal of the American Chemical Society</i>
Manuscript ID:	ja-2013-05511v.R1
Manuscript Type:	Article
Date Submitted by the Author:	03-Aug-2013
Complete List of Authors:	Bell, Franziska; University of California, Berkeley, Department of Chemistry; Lawrence Berkeley National Laboratory, Chemical Sciences Division Ruan, Qiao; Lawrence Berkeley National Laboratory, Chemical Sciences Division Golan, Amir; Lawrence Berkeley National Laboratory, Chemical Sciences Division Horn, Paul; University of California, Berkeley, Department of Chemistry Ahmed, Musahid; Lawrence Berkeley National Laboratory, Chemical Sciences Division Leone, Stephen; University of California, Berkeley, Chemistry Head-Gordon, Martin; University of California, Berkeley, Chemistry

SCHOLARONE™  
Manuscripts

# Dissociative Photoionization of Glycerol and its Dimer Occurs Predominantly via a Ternary Hydrogen-Bridged Ion-Molecule Complex

Franziska Bell,<sup>1,2</sup> Qiao N. Ruan,<sup>2,3</sup> Amir Golan,<sup>2,3</sup> Paul R. Horn,<sup>1,2</sup> Musahid Ahmed,<sup>2</sup> Stephen R. Leone,<sup>2,3</sup> and Martin Head-Gordon<sup>1,2, a)</sup>

<sup>1)</sup> *Department of Chemistry, University of California, Berkeley, California 94720, USA*

<sup>2)</sup> *Chemical Sciences Division, Lawrence Berkeley National Laboratory, Berkeley, California 94720, USA*

<sup>3)</sup> *Departments of Chemistry and Physics, University of California, Berkeley, California 94720, USA*

The photoionization and dissociative photoionization of glycerol are studied experimentally and theoretically. Time-of-flight mass spectrometry (TOF-MS) combined with vacuum ultraviolet (VUV) synchrotron radiation ranging from 8-15 eV is used to investigate the nature of the major fragments and their corresponding appearance energies (AEs). Deuterium (1,1,2,3,3-D5) and <sup>13</sup>C (2-<sup>13</sup>C) labeling is employed to narrow down the possible dissociation mechanisms leading to the major fragment ions (C<sub>3</sub>H<sub>x</sub>O<sub>2</sub><sup>+</sup>, C<sub>2</sub>H<sub>x</sub>O<sub>2</sub><sup>+</sup>, C<sub>2</sub>H<sub>x</sub>O<sup>+</sup>, CH<sub>x</sub>O<sup>+</sup>). We find that the primary fragmentation of the glycerol radical cation (m/z 92) occurs only via two routes. The first channel proceeds via a six-membered hydrogen-transfer transition state, leading to a common stable ternary intermediate, comprised of neutral water, neutral formaldehyde and a vinyl alcohol radical cation, which exhibits a binding energy of ≈ 42 kcal/mol and a very short (1.4 Å) hydrogen bond. Fragmentation of this intermediate gives rise to experimentally observed m/z 74, 62, 44 and 45. Fragments m/z 74 and m/z 62 both consist of hydrogen-bridged ion-molecule complexes with binding energy > 25 kcal/mol, whereas the m/z 44 species lacks such stabilization. This explains why water- or formaldehyde-loss products are observed first. The second primary fragmentation route arises from cleaving the elongated C-C bond. Also for this channel, intermediates comprised of hydrogen-bridged ion-molecule complexes exhibiting binding energies > 24 kcal/mol are observed. Energy decomposition analysis (EDA) reveals that electrostatic and charge-transfer interactions are equally important in hydrogen-bridged ion-molecule complexes. Furthermore, the dissociative photoionization of the glycerol dimer is investigated and compared to the main pathways for the monomeric species. To a first approximation, the glycerol dimer radical cation can be described as a monomeric glycerol radical cation in the presence of a spectator glycerol, thus giving rise to a dissociation pattern similar to that of the monomer.

## I. INTRODUCTION

Glycerol (propane-1,2,3-triol) is widely present in nature as an intermediate in many biological pathways,<sup>1</sup> is ubiquitous in pharmaceutical formulations<sup>2</sup> and furthermore is used as a model system to understand sugar chemistry. Carbohydrates are a major biomass constituent, playing an important role in biology<sup>2</sup> and energy science.<sup>3,4</sup> In particular, the potential of using carbohydrates as biofuels<sup>5</sup> makes their pathways an intensively studied subject.<sup>6-8</sup> The three adjacent hydroxyl groups in glycerol resemble features of the much more complex structure of carbohydrates and their polymeric forms, such as cellulose, and so it is considered a simple model for complex carbohydrates.

So far, both theoretical and experimental work has been aimed at elucidating the pathways involved in the pyrolysis of glycerol,<sup>9-15</sup> with particular focus on the dehydration mechanisms.<sup>11-13</sup> Loss of one or two water molecules in glycerol is facile under these conditions. However due to the presence of three hydroxyl groups

on a relatively flexible carbon backbone many different pathways are possible.<sup>10-13</sup> Since a detailed mechanistic experimental study of glycerol pyrolysis has yet to be carried out, there has been considerable debate in the literature.<sup>9,10</sup>

In particular, more evidence based on real-time analysis and isomeric selectivity is needed to fully understand the pyrolysis mechanism of glycerol. This may be obtained by using synchrotron vacuum ultraviolet (VUV) photoionization, coupled with time-of-flight mass spectrometry (TOF-MS). This approach features several advantages. Firstly, the molecular-beam reduces collision effects and allows unstable intermediates to be isolated. Furthermore, the high energy resolution and tunability of the synchrotron light source minimizes fragmentation and allows different isomers to be distinguished.<sup>16-18</sup> Indeed, recent pyrolytic experiments employing synchrotron VUV photoionization at low pressure, coupled with time-of-flight mass spectrometry (TOF-MS) have given new insights into other combustion mechanisms.<sup>19-21</sup>

However, in order to interpret VUV-TOF-MS data, untangling channels due to pyrolysis from those due to photoionization is necessary. To our knowledge, detailed

<sup>a)</sup> Electronic mail: mhg@cchem.berkeley.edu

1 studies of dissociative photoionization of glycerol in the  
2 VUV region are not yet available and thus such a study  
3 may form the basis of resolving the ongoing debate in  
4 the literature.<sup>9,10</sup>  
5  
6

7 Motivated by this, we investigate the dissociative  
8 photoionization of glycerol using synchrotron radiation  
9 between 8 and 15 eV. Photoionization efficiency (PIE)  
10 curves of the major fragment ions are used to evaluate  
11 the corresponding appearance energies (AEs) resulting  
12 from the dissociative photoionization. The possible  
13 reaction channels for the major fragments are narrowed  
14 down using isotopically labeled samples (1,1,2,3,3-D5  
15 and 2-<sup>13</sup>C glycerol, respectively). Wave-function and  
16 density-functional based calculations are carried out  
17 to characterize the lowest conformers on the radical  
18 cation surface and to further distinguish between the  
19 possible reaction pathways. Furthermore, the dissociative  
20 photoionization of the gas-phase glycerol dimer is  
21 investigated and compared to the proposed pathways for  
22 the monomeric species. Understanding its fragmentation  
23 pathways forms the first step in a series of investigations  
24 involving increasingly complex polyol compounds in  
25 order to elucidate the mechanisms involved in carbohy-  
26 drate chemistry.  
27

28 We find hydrogen-bridged ion-molecule complexes (es-  
29 sentially very strong hydrogen bonding, driven by better  
30 accommodating the net charge) to be a recurring theme  
31 and crucial feature in understanding the photodissocia-  
32 tion pathways of glycerol. In particular, this interaction  
33 causes the experimentally observed appearance energies  
34 for several key fragments to be due to the barrier affil-  
35 iated with the separation of the products rather than the  
36 preceding rearrangement reactions. Furthermore, sev-  
37 eral product fragments are found to feature hydrogen-  
38 bridged ion-molecule interactions, which allow for charge  
39 and spin delocalization between fragments. Hydrogen-  
40 bridged ion-molecule interactions are found to typically  
41 lie between 5 and 35 kcal/mol<sup>22</sup> and are proposed to  
42 play a key role in biology and chemistry, such as pro-  
43 tein folding, enzyme activity,<sup>23,24</sup> biomolecular recog-  
44 nition and sensors,<sup>25</sup> surface adsorption, self-assembly in  
45 supramolecular chemistry and molecular crystals,<sup>26-29</sup>  
46 electrolytes, ion solvation,<sup>30</sup> and ionic clusters.<sup>31-33</sup> In  
47 the context of ionic rearrangements in low-energy radi-  
48 cal species, hydrogen-bridged radical cations, in partic-  
49 ular those containing a O...H...O or N...H...O moiety,  
50 have been proposed to form stable intermediates.<sup>34-37</sup>  
51 Moreover, such observations have not been limited to  
52 the gas phase. For example, a hydrogen-bridged ion has  
53 been proposed to play a key role in the B<sub>12</sub>-catalyzed  
54 dehydration reaction of ethylene glycol.<sup>38</sup> Despite the  
55 apparent importance of such hydrogen-bond mediated  
56 ion-molecule interactions the nature of their bonding is  
57 only poorly understood. In the past, the interaction  
58 was attributed to ion-dipole interactions.<sup>39</sup> However, us-  
59 ing energy-decomposition-analysis (EDA),<sup>40</sup> we are able

to quantify the various components in hydrogen-bridged  
ion-molecule complexes and find that charge-transfer in-  
teractions are equally as important as permanent and  
induced electrostatic effects.

## II. METHODS

### A. Experimental

Experiments are performed on a supersonic molecular  
beam and an effusive beam setup coupled with VUV  
monochromatic radiation. The ionizing VUV radiation  
is provided by a 10 cm period undulator of the Chemical  
Dynamics Beamline at the Advanced Light Source,  
Lawrence Berkeley National Laboratory. The radiation  
is quasi-continuous (70 ps pulses at 500MHz). Higher  
harmonics are filtered out by passing the radiation  
through an argon gas filter. The monochromatized light  
is obtained via a 3 m monochromator with an average  
flux of 10<sup>13</sup> photons per second. Details of the molec-  
ular beam apparatus have been described elsewhere.<sup>41-43</sup>

In the experiment, 50 mg of liquid glycerol (99%  
purity, Sigma Aldrich) without further purification are  
introduced into a 3/8" stainless steel cylindrical nozzle  
with a 100 μm-diameter orifice. The nozzle is heated to  
105°C or 185°C using a cartridge heater to create suffi-  
cient vapor pressure in 50 kPa (150 Torr) of argon before  
the expansion into vacuum. The beam consisting of neu-  
tral monomeric glycerol, as well as clusters then passes  
through a 2 mm-diameter skimmer before it reaches the  
photoionization region. The skimmed molecular beam  
is interrogated by the VUV radiation in the ionization  
region of a TOF reflectron mass spectrometer, where  
1200 V across about 1 cm are applied. If any Rydberg  
states should be populated they would field ionize under  
these conditions and yield characteristic peaks in the  
PIE curve at energies below the adiabatic ionization  
energy. However, no such signature is observed and thus  
their presence can be excluded.

To avoid cluster formation we use an alternative,  
effusive source to introduce the sample into the pho-  
toionization region. The effusive beam is generated by  
thermally vaporizing the sample in an oven attached  
to the repeller plate of the ion optics. The vapors  
then pass through a 1 mm orifice in the plate which  
is located about 1 cm below the interaction region. In  
this case, the experiment is carried out under ambient  
temperatures.

The step size of the VUV photon energy in these  
experiments is 0.10 eV and the data collection time at  
each step is 240 s. The photoionization efficiency (PIE)  
curves are obtained by integrating over the mass peaks  
at each photon energy and normalizing by the photon  
flux measured by a photodiode.

Unlabeled glycerol is obtained from Sigma-Aldrich, whereas the two isotopologue samples, 1,1,2,3,3-D5 glycerol and 2-<sup>13</sup>C glycerol are from Cambridge Isotope Laboratories, Inc.. All glycerol isotopologue samples are nominally 99% isotopically pure and used without further purification.

## B. Computational

Calculations are carried out using a developer's version of Q-Chem 3.2.<sup>44</sup>

*Radical Conformers.* Structures of neutral glycerol given in a recent study<sup>14</sup> are used as a starting point in the geometry optimizations of the radical cation conformers. In order to obtain a quantitative distribution of glycerol conformers, structures are optimized using the Becke, three-parameter, Lee-Yang-Parr exchange correlation functional, B3LYP/6-311++G(p,d),<sup>45</sup> and Møller-Plesset perturbation theory to second order, MP2/6-311++G(p,d). A few conformers indicate considerable changes in geometry upon re-optimization with MP2, a possible indicator for a shallow potential energy surface. Frequency calculations are carried out on all species to confirm local minima. Relative energies are calculated with B3LYP and the range-separated hybrid functional ωB97X<sup>47</sup> with the 6-311++G(2df,2pd) basis, and MP2/aug-cc-pVTZ. For the conformers lowest in energy the complete basis set (CBS) limit is approximated by extrapolation to the MP2/aug-cc-pV(TQ)Z level by using<sup>48</sup>

$$E_{XY} = E_{\text{SCF},Y} + \frac{X^3 E_{\text{CORR},X} - Y^3 E_{\text{CORR},Y}}{X^3 - Y^3}; \quad Y > X \quad (1)$$

where  $X = 3$  and  $Y = 4$  for the  $T \rightarrow Q$  extrapolation. Spin contamination is very low for the radical cation conformers ( $\langle S^2 \rangle_{\text{(B3LYP,}\omega\text{B97X)}} \approx 0.753$ ,  $\langle S^2 \rangle_{\text{(HF)}} \approx 0.775$ ).

*Ionization Energies.* Vertical and adiabatic ionization energies are obtained at different levels of theory, including B3LYP, ωB97X, MP2 and coupled-cluster singles and doubles with perturbative triples correction, (U)CCSD(T),<sup>49,50</sup> with various different basis sets. Details can be found in Tables S 2 and 3 in the Supplementary Information. No frequency corrections are carried out since the adiabatic and vertical geometries are substantially different on the radical cation surface and thus harmonic frequency corrections will yield considerable errors.

*Transition States.* Guesses for the transition state structures are obtained using the freezing string method<sup>51</sup> (B3LYP/6-31G(d)), which requires reactant and product structures as input (unless otherwise indicated, radical cation conformer 100 is used as reactant). Using these guesses, transition states are

then located at the level of B3LYP/6-31+G(p,d) and ωB97X/6-31+G(p,d). Frequency calculations confirm that they lie at a first order saddle point.

The effect of basis set is studied for both B3LYP and ωB97X, by carrying out single point calculations with the considerably larger 6-311++G(2df,p) basis set and the energy variation is found to be 0.19 eV, at the most (Table S 6, Supporting Information). Furthermore, single point calculations using UCCSD(T)/6-31+G(p,d) are carried out using the frozen core approximation. Finally, transition state structures are followed by intrinsic reaction coordinate calculations (IRC)<sup>52</sup> in mass-weighted coordinates toward reactants and products.

*Choice of Functional.* The well-known self-interaction problem<sup>53</sup> may lead to errors in energies and bond lengths when using the still widely popular B3LYP functional. Although self-interaction is not fully resolved in ωB97X,<sup>54</sup> it is known to vastly improve upon B3LYP and has recently been shown to yield an ~ 2.5 smaller average mean unsigned deviation in transition state geometries when tested on the TSG48 set which involves geometrical data on 48 transition states.<sup>55</sup>

*Glycerol Dimer.* Glycerol dimer conformers are obtained by performing a molecular mechanics conformer search in Spartan<sup>56</sup> using the Merck Molecular Force field (MMFF)<sup>57</sup> in combination with three Monte-Carlo runs, each starting from different points and each of which are terminated after 2000 steps. 100 conformers are retained in the simulation. Finally the lowest 50 conformers are selected and re-optimized using B3LYP/6-311++G(p,d).

## III. RESULTS AND DISCUSSION

### A. Experimental Measurements

Figure 1(a) shows the photoionization mass spectrum of glycerol at 10.5 eV in a supersonic beam. The major fragment ions are at  $m/z$  44, 45, 60, 61, 62 and 74. Due to the energetic preference of forming intermolecular rather than intramolecular hydrogen bonds in glycerol, extensive cluster formation occurs in the supersonic expansion process, and ion clusters of various sizes are observed in the mass spectrum. However, no ion clusters are detected under effusive conditions (Figure 1(b)) as a result of the low likelihood of forming glycerol dimers (or higher order clusters) in the vaporization process. The parent signal ( $m/z$  92) is of very low intensity compared to the lower  $m/z$  fragment ions.

Figure 1(c) shows the dissociative photoionization mass spectrum of D5 glycerol using the effusive beam method and a photon energy of 10.5 eV. As expected, the mass spectra of 2-<sup>13</sup>C-glycerol are very similar to the

ones derived from unlabeled glycerol except that almost every peak is shifted one amu higher due to one extra neutron in  $^{13}\text{C}$ .

Figure 2 shows the PIE curves of (a) the parent ion  $\text{C}_3\text{H}_8\text{O}_3^+$  ( $m/z$  92) and the major fragment ions  $\text{C}_3\text{H}_6\text{O}_2^+$  ( $m/z$  74),  $\text{C}_2\text{H}_6\text{O}_2^+$  ( $m/z$  62),  $\text{C}_2\text{H}_4\text{O}^+$  ( $m/z$  44) (b, c, d, respectively). The PIE curves obtained from the supersonic expansion molecular beam and effusive molecular source for a particular fragment ion are rescaled to fit on the same figure for comparison (Figure 2).

The AE for each PIE curve can be determined by using a linear least squares fit in the threshold region<sup>58,59</sup> and are listed in Table 2. The similarity of the PIE curves and corresponding AEs for both types of molecular beams indicates that the photofragment ions with  $m/z < 92$  originate from monomeric glycerol in both experimental settings.

The experimental breakdown diagram is generated by plotting the relative abundance of each fragment ion against photon energy with the sum of the abundance normalized to 1. The breakdown curves corresponding to the dissociation of glycerol are plotted in Figure 3, where only the major fragments are shown for clarity. The fractional abundance of ion  $m/z$  92 decreases while that of fragment ions  $m/z$  74, 62 and 60 rises. This implies that the smaller fragments  $m/z$  74, 62 and 60 derive from the parent fragment  $m/z$  92. Similar analysis for fragments  $m/z$  44 and  $m/z$  45 indicates that these species may originate from  $m/z$  92 or  $m/z$  74 or even both. Moreover the sum of the fractional abundance of  $m/z$  74, 62 and 44 consistently represents around 85% of the total amount of fragment ions over this energy range. This suggests a common intermediate is produced first, which on dissociation (via different pathways) yields the three fragment ions of  $m/z$  74, 62 and 44.

## B. Monomeric Glycerol

### 1. Radical Conformers

An extensive conformer search of neutral glycerol has been carried out previously.<sup>14</sup> For both supersonic and effusive beam experiments, only two neutral conformers (labeled 100 and 95 in the previous study and shown in Figure 4) are thermally accessible.

The calculated *adiabatic* ionization energies for conformers 100 and 95 (9.34 and 9.57 eV, CCSD(T)/aug-cc-pVDZ//B3LYP/6-311++G(p,d)) are in good agreement with the experimentally observed value, which was found to be  $9.4 \pm 0.1$  eV under supersonic conditions. Computed *vertical* ionization energies for various different density functionals and wave-function-based methods and basis sets all lie within a similar range (10.16-10.33

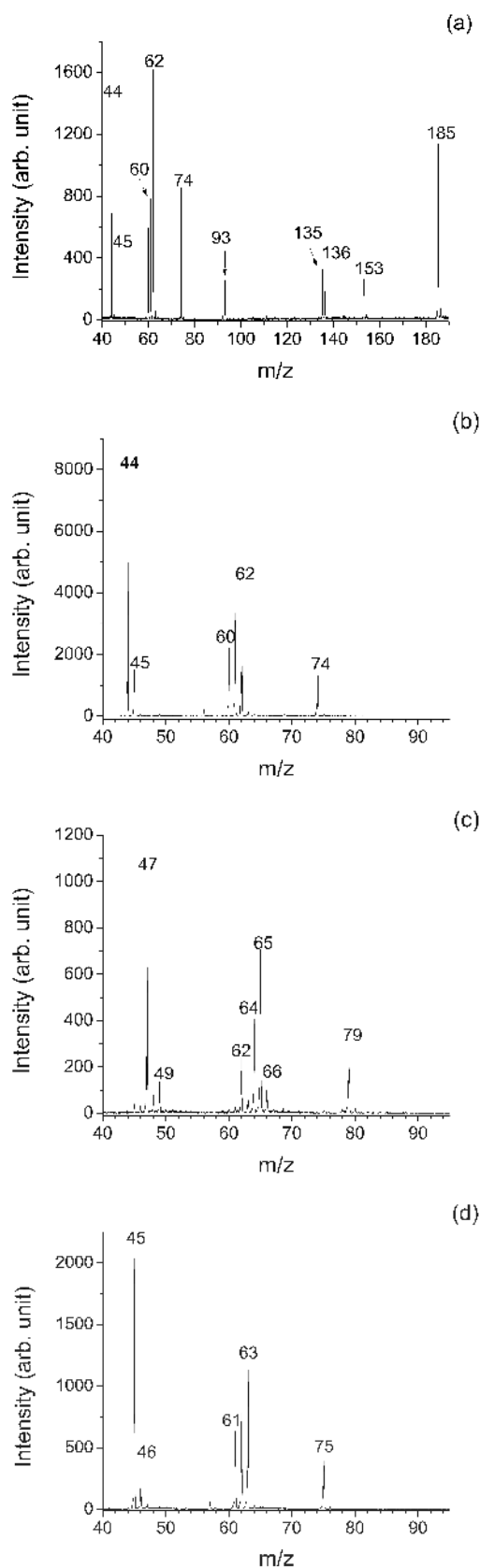


FIG. 1: Photoionization TOF mass spectrum of glycerol in (a) supersonic expansion, (b) effusive source, (c) D5-glycerol, and (d)  $2\text{-}^{13}\text{C}$ -glycerol in an effusive source at 10.5 eV.

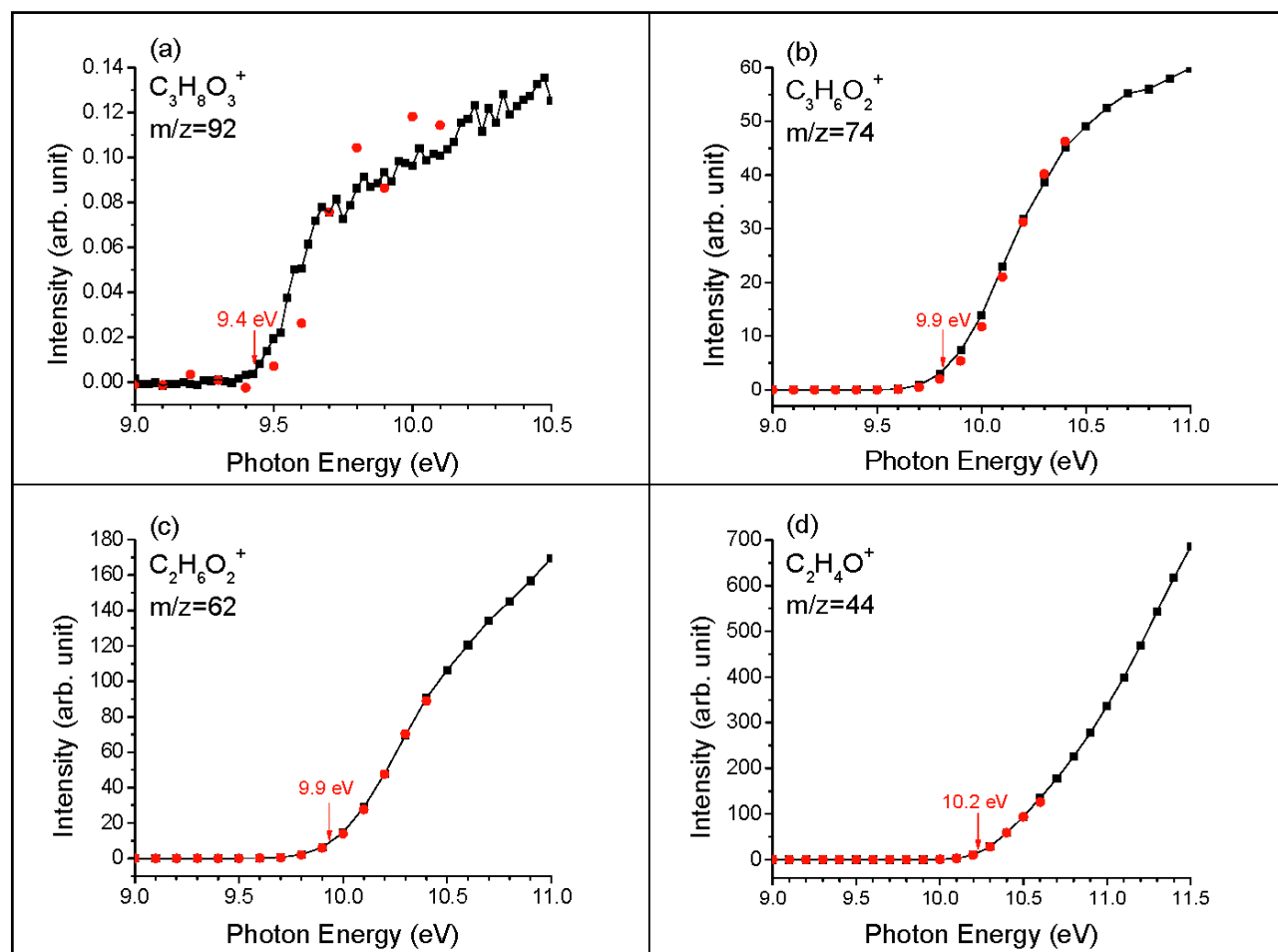


FIG. 2: (a) Normalized PIE curves for the parent ion  $C_3H_8O_3^+$ . The adiabatic IE is found to be  $9.4 \pm 0.1$  eV (supersonic expansion). (b)-(d) Normalized PIE curves for  $C_3H_6O_2^+$ ,  $C_2H_6O_2^+$  and  $C_2H_4O^+$ , respectively. Red circles: supersonic expansion, black rectangles: effusive conditions. AEs shown are from the supersonic expansion.

eV, Table S 2, Supplementary Information).

The vertical ionization energies of conformer 100 and 95 lie at 0.86 eV and 0.93 eV above the corresponding adiabatic transition, respectively (CCSD(T)/aug-cc-pVDZ//B3LYP/6-311++G(p,d)). This leaves the molecule, once ionized, in a vibrationally and rotationally excited state. Due to the presence of this excess energy upon vertical excitation, interconversion between different conformers on the radical cation surface will be facile. Therefore, although the experimental temperature (especially in the supersonic beam experiment) is rather low, most of the conformational surface will be accessible to the radical cation. The results of an extensive conformational search on the radical cation surface is given in the Supplementary Information (Tables S 4 and 5).

Despite the vast number of possible conformers,

they are found to fall into only six subgroups, which are based on their geometrical parameters, such as relative C-C bond lengths and the presence of hydrogen bonds. Geometrical parameters and relative energies of representatives of each of these main sub-classes are given in Table 1, along with the 10 lowest lying conformers. Contrary to chemical intuition, which would predict ionization to occur primarily from the lone pair on the oxygen atoms, all low-lying relaxed radical cation conformers have an extended C-C bond length compared to neutral glycerol. Depending on the conformer under consideration, the extended C-C bond length lies between 1.61 Å and 2.02 Å (Table S 4, Supplementary Information), which is in agreement with previous studies reported on oxygen containing radical cations.<sup>60-63</sup> This behavior was studied in detail for the ethane radical cation,<sup>64</sup> and similarly to this case we expect interconversion between the various conformers to be facile, resulting in the energetically

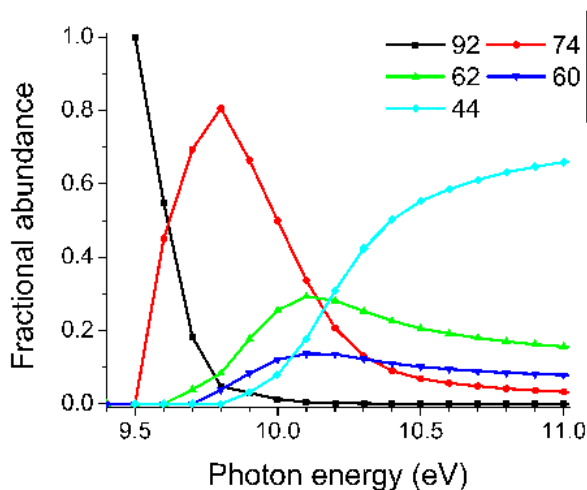


FIG. 3: Overall breakdown diagrams for glycerol in the 9.4 to 11.0 eV photon energy region. The major fragments  $m/z$  92, 74, 62, 60 and 44 are shown.

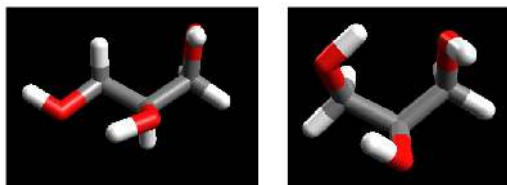


FIG. 4: The energetically two lowest neutral gas-phase conformers. Left: conformer 95, right: conformer 100. C: gray, O: red, H: white.

lowest-lying conformers to actually collapse to one thermally averaged structure.

In order to rule out any channels that may proceed via an electronically excited state of the radical cation, a time-dependent density functional theory (TD-DFT,  $\omega$ B97X/6-311++G(p,d)) calculation was carried out on the vertically ionized glycerol geometry of conformer 100. The lowest optically allowed excitation lies at 10.98 eV with respect to neutral conformer 100.

## 2. Fragmentation Pathways

Figure 5 summarizes the dominant photofragmentation pathways of monomeric glycerol that we find to be consistent with our computations and experimental data. Although many different mechanisms (see Supplementary Information) could give rise to the fragments shown in Figure 5, we find that primary fragmentation of the glycerol radical cation occurs only via two routes.

TABLE 1: Structural features and relative energies (single points, kcal/mol) of representative gas-phase monomeric glycerol radical cation conformers (Conf) for each of the sub-classes, as well as the 10 lowest conformers. O...H lists the shortest hydrogen bond. CT/TT indicates whether the shortest hydrogen bond occurs between a Central and a Terminal (CT) or two Terminal (TT) OH-groups.

Conf	Structural Features B3LYP 6-311++G(p,d)				Rel. Energies	
	O...H (Å)	CT /TT	C-C long(Å)	C-C short(Å)	MP2 /aug-cc-pVTZ	MP2 /T→Q extrap.
75	1.985	TT	1.94	1.51	0.33	
18	2.05	TT	2.01	1.51	2.30	
57	3.11	TT	1.62	1.62	8.18	
100	1.925	CT	1.90	1.51	0.00	0.00
109	1.981	CT	1.96	1.51	-0.57	-0.40
48	1.977	CT	1.96	1.51	-0.60	-1.03
43	1.985	CT	1.96	1.51	-0.58	-0.94
2	1.985	CT	1.96	1.51	-0.58	-0.94
34	1.994	CT	1.98	1.51	-0.68	-1.12
66	1.989	CT	1.98	1.50	-0.68	-1.12
80	1.993	CT	1.98	1.51	-0.71	-1.13
67	1.989	CT	1.98	1.51	-0.68	-1.12
116	3.08	CT	1.95	1.51	2.49	
9	2.60	CT	1.63	1.63	9.41	

The first route involves a low-lying (0.38 eV, Table 2) 6-membered proton-transfer transition state (**TS1**, Figure 5), which is promoted by hydrogen bonding between the two terminal OH groups and the weakened C-C framework caused by ionization. **TS1** leads to a ternary hydrogen-bridged ion-molecule intermediate (**COM1**), comprised of water, formaldehyde and vinyl alcohol radical cation. Fragmentation of this intermediate is found to be responsible for water loss ( $m/z$  74, **COM2**), formaldehyde loss ( $m/z$  62, **COM3**), vinyl alcohol radical cation formation ( $m/z$  44, **P4**) and potentially also formation of fragment ion  $m/z$  45. Although 6-membered transition states are commonly proposed in organic reactions, and for neutral glycerol formation of the vinyl alcohol via such an arrangement was indeed predicted,<sup>11</sup> an intermediate complex composed of two neutral species and a radical cation, such as **COM1**, has not been previously considered in the literature. As will be discussed in the next section, the vinyl alcohol radical cation forms a hydrogen-bridged ion-molecule complex with water and/or formaldehyde. This interaction results in a substantial energy barrier (1.86 eV) to fully separate **COM1** to the individual product fragments **P2** (water), **P3** (formaldehyde) and **P4** (vinyl alcohol radical cation). Similarly, separating **COM1** to produce vinyl radical cation, **P4**, and a hydrogen-bridged complex of neutral water and formaldehyde, **COM4**, requires



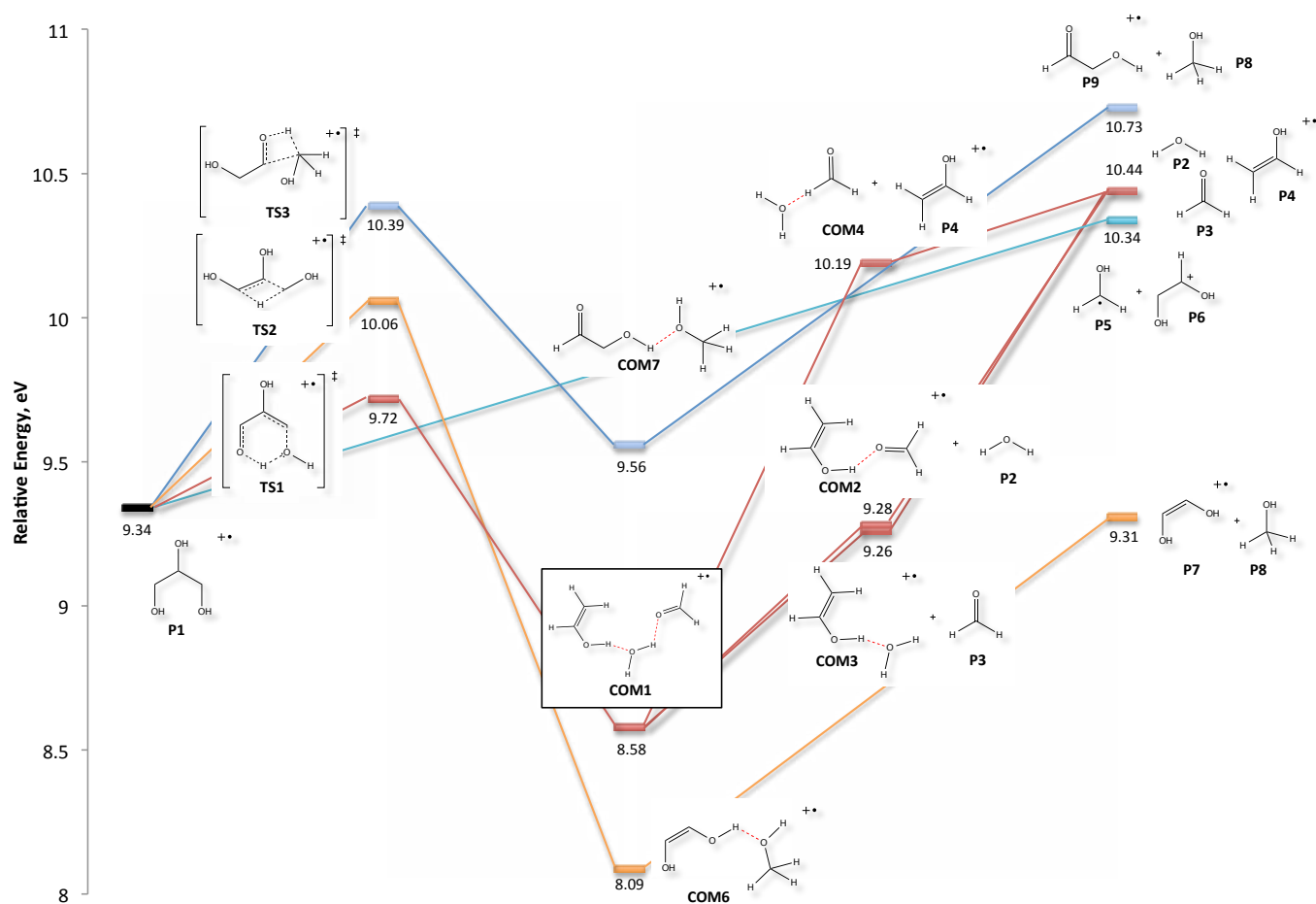


FIG. 5: Summary of the main fragmentation pathways. Energies (in eV) calculated at UCCSD(T)/6-31+G(p,d)// $\omega$ B97X/6-31+G(p,d). The zero of energy is neutral glycerol (conformer 100). TS: transition state, COM: complex, P: product.

1.61 eV. Thus, as a result of the strong ion-molecule interaction the rate-limiting step in the formation of vinyl alcohol radical cation is not the formation of the 6-membered proton-transfer transition state (**TS1**), but rather the separation of the product fragments (Table 2). On the other hand, loss of either neutral water (**P2**) or neutral formaldehyde (**P3**) preserves the strong hydrogen-bridged ion-molecule interaction involving the vinyl alcohol radical cation in the product complex (**COM2**, **COM3**, Figure 5). This accounts for the lower appearance energy for water or, alternatively, formaldehyde loss ( $9.8 \pm 0.1$  and  $9.9 \pm 0.1$  eV, respectively, Table 2) compared to formation of the vinyl alcohol radical cation ( $m/z$  44,  $10.3 \pm 0.1$  eV, Table 2). Indeed, calculations show that the rate limiting step in water (or formaldehyde) loss is the transfer of the proton via the 6-membered transition state (9.72 eV, Table 2). Water (or formaldehyde) separated fully from the product complex lies at only 9.28 eV (9.26 eV) (Table 2). A mechanism via the common intermediate **COM1** also accounts for the similar appearance energies of formaldehyde and water seen in the experiment ( $9.8 \pm 0.1$

and  $9.9 \pm 0.1$  eV, respectively, Table 2). Additionally, the computational prediction of a common intermediate is in accordance with the experimental breakdown diagram presented in Figure 3. Also, since proton transfer occurs between two OH groups, the proposed mechanism via a concerted 6-membered-ring transition state and product complex **COM1** matches the observations in the deuterium labeling experiments (Table 2). Furthermore, the computed AEs arising via **COM1** are in excellent agreement with experimental findings. We have computed a variety of other potential channels and find that they exhibit higher barriers and thus can be excluded. A detailed discussion of these mechanisms can be found in the Supplementary Information. Finally, this mechanism can account for the absence of water- and formaldehyde-loss peaks in the mass spectrum for glycerol dimer, as will be discussed in more detail in section III C.

The second primary fragmentation channel arises from the elongated, and thus weakened, C-C bond in the relaxed radical cation, which is a common feature

TABLE 2: Summary of activation barriers (in eV) and deuterium labeling experiments for the photodissociation of monomeric gas-phase glycerol. Calculations carried out at UCCSD(T)/6-31+G(p,d)// $\omega$ B97X/6-31+G(p,d). Bold: rate-limiting step.

Pathway	Experiment		Calculated
	$\pm 0.1$	D5-glycerol (m/z)	
<b>water loss</b> , m/z 74 6-membered, <b>TS1</b> Prod, <b>COM1+P2</b>	9.8	$C_3HD_5O_2^+$ (79)	<b>9.72</b> 9.28
<b>formald. loss</b> , m/z 62 6-membered, <b>TS1</b> Prod, <b>COM3+P3</b>	9.9	$C_2D_3H_3O_2^+$ (65) $C_2D_4H_2O_2^+$ (66) m/z(65:66)=8:1	<b>9.72</b> 9.26
<b>methanol loss</b> , m/z 60 OH abstr, <b>TS3</b>	10.0	$C_2D_3HO_2^+$ (63) $C_2D_2H_2O_2^+$ (62) m/z(63:62)=2:1	10.39
CH abstr, <b>TS2</b>			<b>10.06</b>
ald prod, <b>P9</b>			10.73
ene-diol prod, <b>P7</b>			9.31
<b>m/z 61</b> Prod, <b>P5+P6</b>	10.3	$C_2D_3H_2O_2^+$ (64)	<b>10.34</b>
<b>vinyl alcohol</b> , m/z 44 6-membered, <b>TS1</b> fully sep prod, <b>P2+P3+P4</b> H <sub>2</sub> O-formald COM, <b>COM4 + P4</b>	10.3	$C_2D_3HO^+$ (47)	9.72 10.44 <b>10.19</b>

in the lowest energy conformers of the ionized glycerol monomer (see section III B 1). This route can result in methanol (**P8**) loss or the loss of a  $CH_2OH$  radical (**P5**) from the parent radical cation (m/z 92), accounting for fragments with m/z 60 (**P7** or **P9**) and 61 (**P6**), respectively. In the case of the cation with m/z 61, loss of a  $CH_2OH$  radical does not feature an exit barrier (see IRC in the Supplementary Information), as is often observed for a radical mechanism of this type. The fully separated products are predicted to lie at 10.34 eV (Table 2), which is in very good agreement with the experimentally observed appearance energy of  $10.3 \pm 0.1$  eV (Table 2). The proposed mechanism is also in agreement with deuterium labeling experiments, which indicate that three of the five C-D are retained in the product. In the case of fragment with m/z 60, we propose two mechanisms, in which the hydrogen atom required to form methanol can either be pulled off the adjacent OH group or the terminal C-H (Figure 5). The former channel yields an aldehyde intermediate (**P9**), whereas the latter yields an ene-diol (**P7**). Deuterium labeling experiments indicate that two products are formed in a ratio of about 2.3:1 (Table 2). The major

product features two deuterium atoms suggesting that abstraction of C-H(D) is favored over dissociation of the hydroxylic proton. Indeed, the calculated barrier for C-H abstraction lies lower than that for O-H abstraction and is found to be in very good agreement with the experimentally measured value (10.06 eV, Table 2).

We also analyzed some of the secondary product fragments, such as fragment m/z 45. Detailed discussions can be found in the Supplementary Information.

### 3. Hydrogen-Bridged Ion-Molecule Interactions

Most fragmentation channels studied in this paper involve highly stable hydrogen-bridged ion-molecule intermediate or product complexes. Such complexes have very strong hydrogen bonds due to the presence of the charge, whose nature we now investigate. Table 3 lists the hydrogen bond lengths and energy decomposition analysis (EDA) terms<sup>40,65</sup> for the binding energy of the molecular species in selected complexes with the radical electron located, in all cases, on the species with the most carbon atoms. The EDA for the neutral water dimer (at the S22 geometry<sup>66</sup>) is also shown for comparison. The binding energies for **COM2**, **COM3**, and **COM7** are exceptionally strong, approximately five times larger than that for the hydrogen bond in the water dimer. One notable difference is the increase in the relative importance of polarization (POL) to charge transfer (CT) from approximately 60% of the charge transfer term in the water dimer to very comparable charge transfer and polarization terms in **COM2**, **COM3**, and **COM7**. The increased fraction of polarization is not surprising for charged systems, since conventional wisdom on these hydrogen-bridged ion-molecule interactions is that they are dominated by polarization. However, our calculations show that charge transfer is still equally important, which is a robust conclusion because the ALMO EDA polarization term is an upper bound to the magnitude of true polarization.<sup>67</sup> Equivalently, the magnitude of the ALMO EDA charge transfer term is a lower bound.

Complementary occupied virtual orbital pair (COVP) analysis<sup>68</sup> in the  $\alpha$  and  $\beta$  spaces for the bimolecular complexes **COM2**, **COM3**, and **COM7** shows that charge transfer is almost exclusively to the radical cation species, with negligible back bonding and, moreover, is roughly symmetric with respect to spin. The approximate symmetry with respect to spin is reasonable given that most of the spin-density of the unpaired electron resides in the C-C bond, which does not participate in the hydrogen-bridged interaction. The most important COVPs for these interactions in the  $\alpha$  space appear in Figure 6 along with the corresponding infinite order perturbation theory charge transfer energy lowerings. It is clear from Figure 6 that the basic lone pair to  $\sigma^*$

charge transfer interaction in the water dimer (a) is also present in **COM2** (b), **COM3** (c), and **COM7** (d).

**COM1** contains vinyl alcohol radical cation, water and formaldehyde with two hydrogen-bonding interactions. The EDA terms for the many body expansion of the cluster to third order (which is exact) are shown in Table 4 along with the EDA of the total interaction of the three species. The interaction energy (INT) is the binding energy neglecting geometric distortion. The dominant two-body term is the vinyl alcohol cation interaction with water ( $E_2[\text{AW}]$ ), which shows a fairly even split between charge transfer and polarization contributions, as was seen above. COVP analysis of this interaction again shows rough spin symmetry for the same reason discussed previously and it reveals that charge donation is primarily from water to the vinyl alcohol radical cation with minimal back donation. The most significant orbital pair with corresponding infinite order perturbation theory charge transfer energy lowering is plotted in Figure 6 (e).

The  $E_2[\text{AF}]$  term corresponding to the interaction between the vinyl alcohol radical cation and formaldehyde is also quite large but different in character. It is predominantly a frozen (FRZ) orbital interaction with a considerably smaller contribution from polarization and negligible charge transfer. Orbital interactions vanish due to the fairly large intermolecular spacing, and the two-body term is largely described by permanent electrostatic interactions between the charged radical cation and the favorably aligned dipole of formaldehyde. The two-body term arising from the interaction of water with formaldehyde ( $E_2[\text{WF}]$ ) is considerably smaller than the other pairwise interactions because only neutral molecules are involved. The EDA reveals a polarization to charge transfer partitioning reminiscent of the neutral water dimer though with an unfavorable frozen term likely due to the contracted hydrogen bond distance. The  $\alpha$  COVP for this pair interaction appears in Figure 6 (f) and, as expected resembles that of the neutral water dimer.

The three-body contribution to the **COM1** interaction energy is comparable to that of the water and formaldehyde pair interaction and primarily polarization and charge transfer in origin with negligible frozen contribution due to the pairwise additivity of permanent electrostatics and minimal overlap of frozen occupied orbitals from all three fragments. The non-negligible polarization and charge transfer terms reflect the fairly large perturbation introduced by a charged species. Analysis of the charge transfer energy lowering for the three-fragment water **COM1** complex by infinite order perturbation theory ( $-17.1$  kcal/mol) shows that 81% of the energy lowering is due to charge transfer from water to the vinyl alcohol radical cation, and 16% is due to charge transfer from formaldehyde to water, and there

TABLE 3: Hydrogen bond lengths and ALMO Energy Decomposition Analysis terms and binding energies for selected complexes and the S22 water dimer for  $\omega\text{b97x}/6\text{-311++G}(2\text{df},2\text{pd})$  in kcal/mol.

Complex	FRZ	POL	CT	BIND	$R_{\text{HB}}(\text{\AA})$
$(\text{H}_2\text{O})_2$	-3.19	-0.92	-1.51	-5.62	1.952
<b>COM2</b>	-4.36	-12.88	-12.17	-26.77	1.487
<b>COM3</b>	-6.19	-10.37	-11.29	-25.80	1.491
<b>COM7</b>	-2.67	-12.32	-12.60	-24.33	1.412

TABLE 4: Hydrogen bond lengths and ALMO Energy Decomposition Analysis terms for the many body (MB) expansion of the **COM1** binding energy for  $\omega\text{b97x}/6\text{-311++G}(2\text{df},2\text{pd})$  in kcal/mol. A indicates the vinyl alcohol radical cation, W indicates water, and F indicates formaldehyde.  $E_2$  and  $E_3$  are two- and three-body terms, respectively.

MB Term	FRZ	POL	CT	INT	BIND	$R_{\text{HB}}(\text{\AA})$
$E_2[\text{AW}]$	2.81	-14.87	-16.45	-28.51	-	1.382
$E_2[\text{AF}]$	-10.33	-2.09	-0.36	-12.78	-	-
$E_2[\text{WF}]$	1.47	-1.53	-2.84	-2.91	-	1.750
$E_3[\text{AWF}]$	-0.17	-1.99	-1.24	-3.40	-	-
TOT	-6.23	-20.48	-20.89	-47.59	-41.79	-

is again minimal charge transfer between vinyl alcohol cation and formaldehyde. Perhaps most interestingly, the infinite order perturbation theory charge transfer energy lowering from the three-body term is dominated by fairly equal parts water to vinyl alcohol radical cation and formaldehyde to water charge donation to stabilize the cation.

### C. Glycerol Dimer

Since glycerol is known to form extensive intermolecular hydrogen bonding networks,<sup>69-71</sup> we were interested in how the dissociative channels are influenced by the presence of a second glycerol molecule. Moreover, understanding its fragmentation pathways forms the first step in a series of investigations involving increasingly complex polyol compounds in order to elucidate the mechanisms involved in carbohydrate chemistry.

A conformer search for neutral glycerol dimer was carried out (see section IIB for details). The lowest structure is displayed in Figure 7, and lies 0.71 eV ( $\omega\text{B97X}/6\text{-311++G}(p,d)//\text{B3LYP}/6\text{-311++G}(p,d)$ ) below two isolated neutral monomeric glycerol molecules (conformer 100). Table 5 summarizes the relative energies and some structural parameters of the lowest 10 dimer conformers. The low-lying structures feature mainly intermolecular rather than intramolecular hydro-

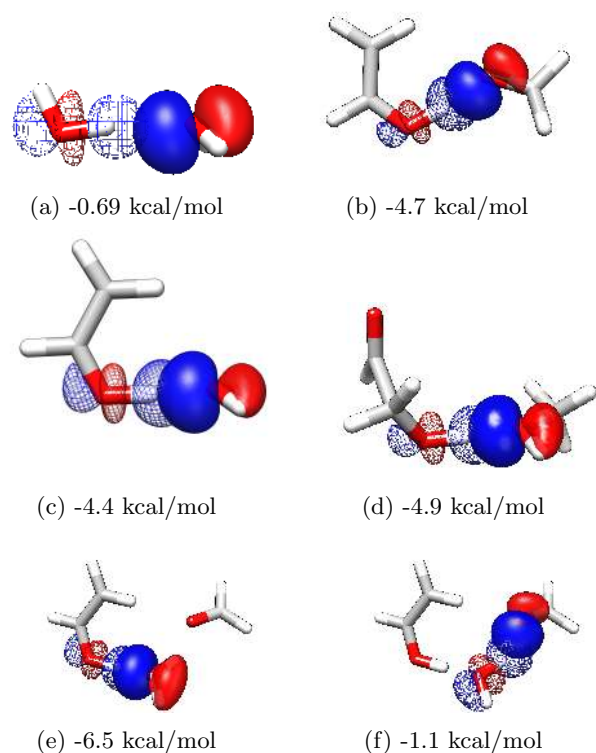


FIG. 6: Complementary Occupied Virtual orbital Pairs (COVOPs) for (a) the water dimer, (b) **COM2**, (c) **COM3**, (d) **COM7**, (e) **COM1** vinyl alcohol radical cation and water, (f) **COM1** vinyl alcohol radical cation and formaldehyde. The virtual orbital of the pair is depicted as mesh. All orbital pairs and energy lowerings (kcal/mol) are for the  $\alpha$  space. The orbitals and corresponding energy lowerings in the beta space are roughly the same (identical for restricted (a) and (f)) because the radical electron is in the C-C bond and does not directly participate in the hydrogen-bridged interactions.

gen bonds. This is not surprising, as the directionality and distance of intramolecular hydrogen bonds are not as favorable. For the two lowest structures both intramolecular hydrogen bonds are between the two terminal OH groups, which allows each of the glycerol molecules to adopt a chair-like conformation.

Upon ionization, almost the entire spin density (Figure 8) is located on one of the glycerol molecules and so a similar trend in geometric parameters as for monomeric glycerol radical cation is observed, i.e. one of the C-C bonds is extended considerably (to 1.83 Å) (Table 6). The finding that the glycerol dimer radical cation can, to a first approximation, be described as a monomeric glycerol radical cation in the presence of a spectator glycerol, suggests that the dissociative photoionization pathways observed should resemble those of the monomeric species. Indeed, just as for

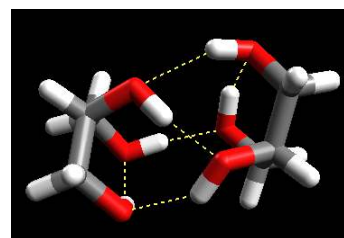
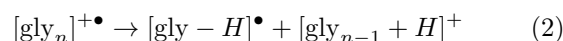


FIG. 7: Cartoon of the lowest energy dimer structure (conformer 1), highlighting the hydrogen bonding network.

the monomeric radical cation, fragment ions resulting from the loss of  $m/z$  31 (attributed to hydroxymethyl radical) and  $m/z$  48 (assigned to the loss of neutral water and formaldehyde) are observed for the glycerol dimer radical cation (Table 7). Furthermore, proton transfer via a six-membered transition state (analogous to Figure 5) is expected to be very facile due to the hydrogen bonding network that favors intramolecular hydrogen bonds between the two terminal OH groups. This is supported by the appearance energy observed for fragment  $m/z$   $(184 - 48) = m/z$  136 (9.6 eV, Table 7), which lies close in energy to the 9.72 eV barrier computed for the concerted 6-membered dissociation of monomeric glycerol (Table 2).

However, in contrast to monomeric glycerol, the presence of a spectator glycerol molecule is expected to considerably lower the barrier affiliated with separating the resulting products of this reaction (e.g. water, formaldehyde and the vinyl alcohol radical cation) as it aids the delocalization of positive charge and spin density. This could explain why, contrary to monomeric glycerol, no  $m/z$   $(184 - 18)$  (water loss) or  $m/z$   $(184 - 30)$  (formaldehyde loss) peaks are observed in the mass spectrum of the glycerol dimer radical cation (Table 7), but rather dissociation into three product fragments occurs. The other main difference to monomeric glycerol radical cation is the presence of  $M+1$  peaks in the mass spectrum of clustered glycerol species, such as  $m/z$  93 and  $m/z$  185. These correspond to protonated monomeric and dimeric glycerol, respectively. We propose that these protonated species occur from  $H^\bullet$  transfer within  $(\text{glycerol})_n$  radical cation species, followed by dissociation of the cluster into fragments, as follows:



Here,  $[\text{gly} - H]^\bullet$  denotes a glycerol molecule from which a hydrogen atom is abstracted.

Although such a process is highly unlikely in an uncharged species (c.f. the  $pK_a$  value of an OH group in glycerol), ionization makes this process feasible. The

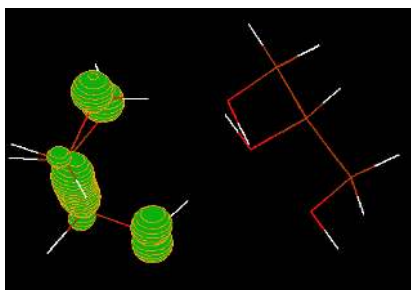


FIG. 8: Spin density in glycerol dimer radical cation (cutoff: 0.02).

TABLE 5: Relative energies (in kcal/mol) and key structural parameters for the ten lowest energy gas-phase glycerol dimer conformers. Structures were optimized at the B3LYP/6-311++G(p,d) level of theory. The type of hydrogen bond is indicated by TT (between the two terminal OH groups or CT (between a terminal and a central OH group).

Conf	Rel. E		No. of H bonds	
	$\omega$ B97X/6-311++G(p,d)	B3LYP	(No. of intra. H bonds, type)	
			< 2.0Å	< 2.5Å
1	0.00	0.00	4 (2, TT)	6 (2, TT)
2	0.09	-0.04	5 (2, TT)	6 (2, TT)
3	1.10	1.45	5 (1, TT)	6 (2, TT, CT)
4	1.11	0.83	5 (1, TT)	6 (2, TT, CT)
5	1.49	1.33	5 (1, TT)	6 (2, TT, CT)
6	1.89	2.02	5 (1, TT)	6 (2, TT, CT)
7	1.96	1.98	5 (1, TT)	6 (2, TT, CT)
8	2.07	2.01	5 (1, TT)	6 (2, TT, CT)
9	2.09	2.02	5 (1, TT)	6 (2, TT, CT)
10	2.44	2.59	5 (1, TT)	6 (2, TT, CT)

products for reaction (2) with  $n = 2$ , for example, lie at 9.56 eV ( $\omega$ B97X/6-311++G(p,d)//B3LYP/6-311++G(p,d)) with respect to two neutral isolated glycerol molecules (conformer 100).

Since the AE for the protonated glycerol dimer cation ( $m/z$  185) lies above the AEs of fragment ions with  $m/z$  153, 136 and 135 this suggests that these photodissociation products arise from the unprotonated glycerol dimer radical cation ( $m/z$  184).

#### IV. CONCLUSIONS

In this study, the dissociative photoionization of glycerol and glycerol dimer is investigated both experimentally and theoretically. Low pressure conditions combined with tunable synchrotron radiation and time-of-flight mass spectrometry allow appearance energies of radical species to be determined with high-energy resolution. Glycerol is found to have a very high tendency to

TABLE 6: Key structural parameters for gas-phase glycerol dimer radical cation, conformer 1. Radical cation indicates the glycerol molecule that displays most of the spin density in the dimer. TT O...H is the hydrogen bond distance between the two terminal OH groups.

	C-C long Å	C-C short Å	TT O...H Å
radical cation	1.83	1.53	2.34
neutral	1.53	1.52	1.83

TABLE 7: Appearance energies (AEs) (in eV  $\pm 0.1$ ) measured in the dissociative photoionization of glycerol between 93  $m/z$  and 185  $m/z$  (supersonic beam).

Ion ( $m/z$ ) <sup>a</sup>	Fragment(s) lost ( $m/z$ )	AEs
		(eV)
$[\text{C}_3\text{H}_8\text{O}_3 + \text{H}]^+$ (93)	91	10.5
$[\text{C}_3\text{H}_8\text{O}_3 + \text{C}_2\text{H}_2\text{O}]^+$ (135)	49	10.0
$[\text{C}_3\text{H}_8\text{O}_3 + \text{C}_2\text{H}_3\text{O}]^+$ (136)	48	9.7
$[\text{C}_3\text{H}_8\text{O}_3 + \text{C}_2\text{H}_5\text{O}_2]^+$ (153)	31	9.5
$[\text{C}_3\text{H}_8\text{O}_3 + \text{C}_3\text{H}_9\text{O}_3]^+$ (185)	91	9.9

<sup>a</sup> No glycerol dimer cation ( $m/z$  184) is detected above the background noise. However, contrary to the parent glycerol monomer cation ( $m/z$  92), the photon energy step size was not decreased and the collection time not increased when recording the mass spectrum in the region of  $m/z$  184.

fragment upon photoionization, which we find is due to the weakened carbon framework in the glycerol radical cation. Its lowest barrier to rearrangement is a six-membered transition structure leading to a stable ternary intermediate complex (**COM1**) composed of formaldehyde, water and vinyl alcohol radical cation, with an energy about 0.75 eV below glycerol cation.

Due to the presence of strong hydrogen-bridged ion-molecule interactions, full separation of the three components in **COM1** is energetically unfavorable and explains why either water- or formaldehyde-loss products are observed at lower appearance energies experimentally. We also elucidate detailed mechanisms leading to fragments that are observed at higher energies, such as the loss of methanol and hydroxymethyl radical, and show that these arise as a result of the weakened C-C bond upon ionization.

In several fragmentation channels the observed appearance energy is due to energy cost of separating the product fragments from one another rather than the rearrangements to the product complex. This is because the intermediates exhibit very strong ( $> 25$  kcal/mol) hydrogen-bridged ion-molecule interactions. In addition, several product fragments were themselves identified as ion-molecule complexes, involving similarly strong

hydrogen-bridged ion-molecule interactions, making such interactions one of the recurring themes in this study. Whilst they have been previously attributed to ion-dipole interactions, we perform an energy decomposition analysis of the complexes, which reveals that about half the interaction energy is associated with charge-transfer.

In a first attempt to understand the fragmentation pathways in complex polyols and carbohydrates, we also studied the dissociative photoionization of glycerol dimer. Our studies suggest that the glycerol dimer radical cation can be viewed, to a first approximation, as a monomeric glycerol cation in the presence of a spectator molecule and therefore exhibits similar photodissociation pathways to monomeric glycerol. The main difference is the absence of a water- and formaldehyde loss peak, which we propose to be due to the spectator glycerol molecule. Its presence causes a lowering in the product dissociation barrier and allows more facile separation of the three fragments. Due to the structural resemblance between glycerol dimer and simple carbohydrates, these results suggest that carbohydrates should exhibit similar rich fragmentation patterns.

The combined use of electronic structure calculations with synchrotron based mass spectrometry promises to be a powerful tool in elucidating the molecular decomposition pathways of systems relevant to energy conversion processes.

## V. ACKNOWLEDGMENTS

The experiments were carried out at the Advanced Light Source at Lawrence Berkeley National Laboratory; LBNL participants are supported by the Office of Science, Office of Basic Energy Sciences, Office of the US Department of Energy under Contract No. DE-AC02-05CH11231, through the Chemical Sciences Division (F.B., A.G., P.R.H., S.R.L., M.A., M.H.G.).

## VI. SUPPORTING INFORMATION AVAILABLE

Supplementary experimental data. Glycerol radical cation conformer study. Alternative Mechanisms. This information is available free of charge via the internet at <http://pubs.acs.org>

## VII. REFERENCES

- <sup>1</sup>F. REMIZE, L. BARNAVON, and D. S., *Metab. Eng.* **3**, 301 (2001).
- <sup>2</sup>K. C. NICOLAOU and H. J. MITCHELL, *Angew. Chem. International Edition* **40**, 1576 (2001).
- <sup>3</sup>J. J. BOZELL, *Chemicals and Materials from Renewable Resources*, volume 784, 2001.
- <sup>4</sup>R. RUHAL, S. AGGARWAL, and B. CHOUDHURY, *Green Chem.* **13**, 3492 (2011).
- <sup>5</sup>G. W. HUBER, S. IBORRA, and A. CORMA, *Chem. Rev.* **106**, 40444098 (2006).
- <sup>6</sup>J. B. PAINE, III, Y. B. PITHAWALLA, and J. D. NAWORAL, *Journal of Analytical and Applied Pyrolysis* **82**, 10 (2008).
- <sup>7</sup>J. B. PAINE, III, Y. B. PITHAWALLA, and J. D. NAWORAL, *Journal of Analytical and Applied Pyrolysis* **82**, 42 (2008).
- <sup>8</sup>J. B. PAINE, III, Y. B. PITHAWALLA, and J. D. NAWORAL, *Journal of Analytical and Applied Pyrolysis* **83**, 37 (2008).
- <sup>9</sup>M. STEIN, Y.S. AND ANTAL and M. J. JONES, *Journal of Analytical and Applied Pyrolysis* **4**, 283 (1983).
- <sup>10</sup>J. B. PAINE, III and C. THOMAS, JR., *Journal of Analytical and Applied Pyrolysis* **80**, 297 (2007).
- <sup>11</sup>M. NIMLOS, S. BLANKSBY, X. QIAN, M. E. HIMMEL, and D. JOHNSON, *J. Phys. Chem. A* **110**, 6145 (2006).
- <sup>12</sup>W. SUN, J. LIU, X. CHU, C. ZHANG, and C. LIU, *J. Mol. Struct.: THEOCHEM* **942**, 38 (2010).
- <sup>13</sup>T. LAINO, C. TUMA, A. CURIONI, E. JOCHNOWITZ, and S. STOLZ, *J. Phys. Chem. A* **115**, 3592 (2011).
- <sup>14</sup>C. S. CALLAM, S. J. SINGER, T. L. LOWARY, and C. M. HADAD, *J. Am. Chem. Soc.* **123**, 11743 (2001), PMID: 11716731.
- <sup>15</sup>R. CHELLI, F. L. GERVASIO, C. GELLINI, P. PROCACCI, G. CARDINI, and V. SCETTINO, *J. Phys. Chem. A* **104**, 11220 (2000).
- <sup>16</sup>T. A. COOL, K. NAKAJIMA, T. A. MOSTEFAOUI, F. QI, A. MCLILROY, P. R. WESTMORELAND, M. E. LAW, L. POISSON, D. S. PETERKA, and M. AHMED, *J. Chem. Phys.* **119**, 8356 (2003).
- <sup>17</sup>T. A. COOL, K. NAKAJIMA, C. A. TAATJES, A. MCLILROY, P. R. WESTMORELAND, and M. E. LAW, *Proc. Combust. Inst.* **30**, 1681 (2005).
- <sup>18</sup>N. HANSEN, C. A. KLIPPENSTEIN, S. J. TAATJES, J. A. MILLER, J. WANG, T. A. COOL, B. YANG, L. X. WEI, C. Q. HUANG, J. WANG, F. QI, M. E. LAW, and P. R. WESTMORELAND, *J. Phys. Chem. A* **110**, 3670 (2006).
- <sup>19</sup>Y. LI and F. QI, *Acc. Chem. Res.* **43**, 68 (2010).
- <sup>20</sup>K. KOHSE-HOEINGHAUS, P. OSSWALD, T. A. COOL, T. KASPER, N. HANSEN, F. QI, C. K. WESTBROOK, and P. R. WESTMORELAND, *Angew. Chem. Int. Ed.* **49**, 3572 (2010).
- <sup>21</sup>C. A. TAATJES, N. HANSEN, D. L. OSBORN, K. KOHSE-HOEINGHAUS, T. A. COOL, and P. R. WESTMORELAND, *Phys. Chem. Chem. Phys.* **10**, 20 (2008).
- <sup>22</sup>M. MEOT-NER (MAUTNER), *Chem. Rev.* **105**, 213 (2005).
- <sup>23</sup>C. N. FURHMANN, M. D. DAUGHERTY, and D. A. AGARD, *J. Am. Chem. Soc.* **128**, 9086 (2006).
- <sup>24</sup>A. DAS, S. MAHALE, V. PRASHAR, S. BIHANI, J.-L. FERRER, and M. V. HOSUR, *J. Am. Chem. Soc.* **132**, 6366 (2010).
- <sup>25</sup>Z. XU, N. J. SINGH, J. LIM, J. PAN, H. N. KIM, S. PARK, K. S. KIM, and J. YOON, *J. Am. Chem. Soc.* **131**, 15528 (2009).
- <sup>26</sup>D. PAYER, A. COMISSO, A. DMITRIEV, T. STRUNSKUS, N. LIN, C. WOELL, A. DEVITA, J. V. BARTH, and K. KERN, *Chem. Eur. J.* **13**, 3900 (2007).
- <sup>27</sup>L. BRAMMER, J. K. SWEARINGER, B. E. A., and P. SHERWOOD, *PNAS* **99**, 4956 (2002).
- <sup>28</sup>H. FENNIRI, P. MATHIVANAN, K. L. VIDALE, D. M. SHERMAN, K. HALLENGA, K. V. WOOD, and J. G. STOWELL, *J. Am. Chem. Soc.* **123**, 3854 (2001).
- <sup>29</sup>C. V. KRISHNAMOHAN-SHARMA and A. CLEARFIELD, *J. Am. Chem. Soc.* **122**, 4394 (2000).
- <sup>30</sup>P. AYOTTE, C. G. BAILEY, G. H. WEDDLE, and M. A. JOHNSON, *J. Phys. Chem. A* **102**, 3067 (1998).
- <sup>31</sup>M. CASTRO, *J. Phys. Chem. A* **116**, 5529 (2012).
- <sup>32</sup>J. S. PRELL and E. R. WILLIAMS, *J. Am. Chem. Soc.* **131**, 4110 (2009).
- <sup>33</sup>Y.-S. WANG, H.-C. CHANG, J.-C. JIANG, S. H. LIN, Y. T. LEE, and H.-C. CHANG, *J. Am. Chem. Soc.* **120**, 8777 (1998).
- <sup>34</sup>J. K. TERLOUW and P. C. BURGERS, *Encyclopedia of mass Spectrometry*, volume 4, Elsevier:Amsterdam, 2005.
- <sup>35</sup>J. K. TERLOUW, W. HEERMA, P. C. BURGERS, and J. L. HOLMES, *Can. J. Chem.* **62**, 289 (1984).
- <sup>36</sup>D. SUB, P. C. BURGER, and J. K. TERLOUW, *Rapid Commun.*



- 1  
2  
3  
4  
5  
6  
7  
8  
9  
10  
11  
12  
13  
14  
15  
16  
17  
18  
19  
20  
21  
22  
23  
24  
25  
26  
27  
28  
29  
30  
31  
32  
33  
34  
35  
36  
37  
38  
39  
40  
41  
42  
43  
44  
45  
46  
47  
48  
49  
50  
51  
52  
53  
54  
55  
56  
57  
58  
59  
60
- Mass Spectrom.* **9**, 862 (1995).
- <sup>37</sup>K. J. JOBST and M. A. TRIKOUPIS, *Eur. J. Mass Spectrom.* **18**, 183 (2012).
- <sup>38</sup>M. FELIKS and G. M. ULLMANN, *J. Phys. Chem. B* **116**, 7076 (2012).
- <sup>39</sup>J. HURSAK, G. A. MCGIBBON, H. SCHWARZ, and J. K. TERLOUW, *Int. J. Mass Spectr.* **160**, 117 (1997).
- <sup>40</sup>P. R. HORN, E. J. SUNDSTROM, T. A. BAKER, and M. HEAD-GORDON, *J. Chem. Phys.* **138**, 134119 (2013).
- <sup>41</sup>C. NICOLAS, J. N. SHU, D. S. PETERKA, M. HOCHLAF, L. POISSON, S. R. LEONE, and M. AHMED, *J. Am. Chem. Soc.* **128**, 220 (2006).
- <sup>42</sup>O. KOSTKO, L. BELAU, K. R. WILSON, and M. AHMED, *J. Phys. Chem. A* **112**, 9555 (2008).
- <sup>43</sup>L. BELAU, K. R. WILSON, S. R. LEONE, and M. AHMED, *J. Phys. Chem. A* **111**, 7562 (2007).
- <sup>44</sup>Y. SHAO et al., *Phys. Chem. Chem. Phys.* **8**, 3172 (2006).
- <sup>45</sup>A. D. BECKE, *J. Chem. Phys.* **98**, 1372 (1993).
- <sup>46</sup>C. MÖLLER and M. S. PLESSET, *Phys. Rev.* **46**, 618 (1934).
- <sup>47</sup>J.-D. CHAI and M. HEAD-GORDON, *J. Chem. Phys.* **131**, 174105 (2009).
- <sup>48</sup>A. HALKIER, T. HELGAKER, P. JØRGENSEN, W. KLOPPER, H. KOCH, J. OLSEN, and A. K. WILSON, *Chem. Phys. Lett.* **286**, 243 (1998).
- <sup>49</sup>K. RAGHAVACHARI, G. W. TRUCKS, J. A. POPLE, and M. HEAD-GORDON, *Chem. Phys. Lett.* **157**, 479 (1989).
- <sup>50</sup>M. URBAN, J. NOGA, S. J. COLE, and R. J. BARTLETT, *J. Chem. Phys.* **83**, 4041 (1985).
- <sup>51</sup>A. BEHN, P. M. ZIMMERMAN, A. T. BELL, and M. HEAD-GORDON, *J. Chem. Phys.* **135**, 224108 (2011).
- <sup>52</sup>K. FUKUI, S. KATO, and H. FUJIMOTO, *J. Am. Chem. Soc.* **97**, 1 (1975).
- <sup>53</sup>J. P. PERDEW and A. ZUNGER, *Phys. Rev. B* **23**, 5048 (1981).
- <sup>54</sup>J.-D. CHAI and M. HEAD-GORDON, *J. Chem. Phys.* **131**, 174105 (2009).
- <sup>55</sup>X. XU, I. M. ALECU, and D. G. TRUHLAR, *Journal of Chemical Theory and Computation* **7**, 1667 (2011).
- <sup>56</sup>Spartan08 Wavefunction Inc. Irvine, CA.
- <sup>57</sup>T. A. HALGREN, *J. Comp. Chem.* **17**, 490 (1996).
- <sup>58</sup>K. R. WILSON, L. BELAU, C. NICOLAS, M. JIMENEZ-CRUZ, S. R. LEONE, and M. AHMED, *Int. J. Mass Spectrom.* **155**, 249 (2006).
- <sup>59</sup>J. C. TRAEGER and B. W. KOMPE, *Int. J. Mass Spectrom. Ion Processes* **101**, 111 (1990).
- <sup>60</sup>J. W. GAULD and L. RADOM, *Chem. Phys. Lett.* **275**, 28 (1997).
- <sup>61</sup>D. GHOSH, A. GOLAN, L. K. TAKAHASHI, A. I. KRYLOV, and M. AHMED, *J. Phys. Chem. Lett.* **3**, 97 (2012).
- <sup>62</sup>D. J. BELLVILLE and N. L. BAULD, *J. Am. Chem. Soc.* **104**, 5700 (1982).
- <sup>63</sup>D. J. BELLVILLE, R. A. PABON, and N. L. BAULD, *J. Am. Chem. Soc.* **107**, 4978 (1985).
- <sup>64</sup>H. M. SULZBACH, D. GRAHAM, S. J. C., and H. F. SCHAEFER, III, *Acta Chemica Scandinavica* **51**, 547 (1997).
- <sup>65</sup>R. Z. KHALIULLIN, E. COBAR, R. LOCHAN, A. T. BELL, and M. HEAD-GORDON, *J. Phys. Chem. A* **111**, 8753 (2007).
- <sup>66</sup>P. JURECKA, J. SPONER, J. CERNY, and P. HOBZA, *Phys. Chem. Chem. Phys.* **8**, 1985 (2006).
- <sup>67</sup>R. AZAR, P. R. HORN, E. J. SUNDSTROM, and M. HEAD-GORDON, *J. Chem. Phys.* **138**, 084102 (2013).
- <sup>68</sup>R. Z. KHALIULLIN, A. T. BELL, and M. HEAD-GORDON, *J. Chem. Phys.* **128**, 184112 (2008).
- <sup>69</sup>R. CHELLI, P. PROCACCI, G. CARDINI, and S. CALIFANO, *Phys. Chem. Chem. Phys.* **1**, (1999).
- <sup>70</sup>D. CHAMPENEY, R. JOARDER, and J. DORE, *Mol. Phys.* **58**, 337 (1986).
- <sup>71</sup>R. BOHMER and G. HINZE, *J. Chem. Phys.* **109**, 241 (1998).

